An Implementation of the Robust Inviscid Wall Boundary Condition in High-Speed Flow Calculations

Moon-Sang Kim*†
Associate Professor, School of Aerospace and Mechanical Engineering, Hankuk Aviation University
Byung-Woo Jeon, Yong-Nyun Kim
Research Assistant, Department of Aerospace Engineering, Hankuk Aviation University
Hyeok-Bin Kwon
Research Assistant, Department of Aerospace Engineering, Institute of Advanced Machinery Design, Seoul National University
Dong-Ho Lee
Professor, School of Mechanical and Aerospace Engineering, Seoul National University

Boundary condition is one of the major factors to influence the numerical stability and solution accuracy in numerical analysis. One of the most important physical boundary conditions in the flowfield analysis is the wall boundary condition imposed on the body surface. To solve a two-dimensional Euler equation, totally four numerical wall boundary conditions should be prescribed. Two of them are supplied by the flow tangency condition. The other two conditions, therefore, should be prepared additionally in a suitable way. In this paper, four different sets of wall boundary conditions are proposed and then applied to solve high-speed flowfields around a quarter circle geometry. A two-dimensional compressible Euler solver is prepared based on the finite volume method. This solver hires three different upwind schemes; Steger-Warming's flux vector splitting, Roe's flux difference splitting, and Liou's advection upstream splitting method. It is found that the way to specify the additional numerical wall boundary conditions strongly affects the overall stability and accuracy of the upwind schemes in high-speed flow calculation. The optimal wall boundary conditions should be also chosen very carefully depending on the numerical schemes used to solve the problem.

Key Words : Wall Boundary Condition, Upwind Scheme, High-Speed Flow

Nomenclature

a : Speed of sound
E : Total energy per unit mass
F : x-directional convection term
G : y-directional convection term
H : Total enthalpy per unit mass
M : Mach number
p : Pressure
Q : Conservative variables
S : Eigenvector matrix
u : x-directional velocity component
v : y-directional velocity component
α : Angle of attack
γ : Specific heat ratio
Λ : Eigenvalue matrix
λ : Eigenvalue
ρ : Air density
$(\cdot)_R$: Variable quantity at node point $(i+1)$
$(\cdot)_L$: Variable quantity at node point (i)

† First Author
* Corresponding Author,
E-mail : mskim@mail.hangkong.ac.kr
TEL : +82-2-300-0285; **FAX** : +82-2-3158-2191
Hwajon-dong, Deokyang-ku, Koyang, Kyunggi-do 412-791, Korea.(Manuscript **Received** December 18, 2000; **Revised** March 9, 2001)

1. Introduction

In any numerical algorithm, the boundary

conditions play a crucial role in both the stability and accuracy of the numerical scheme. Even though the numerical scheme (Moretti 1979, Chakravarthy et al. 1980, Steger and Warming 1981, Roe 1981, Liou 1996, Cho 1997, and Kim et al. 1998) is very prominent, appropriate boundary conditions should be prepared to have physically correct and numerically accurate solutions. The boundary conditions can be implemented after the system of partial differential equations and the types of physical boundaries are specified. Once the physical configuration is specified, the physical boundary conditions are expressed in terms of mathematical conditions. Then these conditions are approximated numerically.

One of the most important physical boundary conditions in the flowfield analysis is the wall boundary condition on the body surface. The flow tangency condition is necessary to designate the body surface in the inviscid flow. However, this is not a sufficient wall boundary condition to solve a two-dimensional compressible Euler equation because Euler equation is composed of four non-linear partial differential equations; mass conservation equation, two momentum equations, and energy equation. Therefore, totally four inviscid wall boundary conditions should be prescribed to solve an Euler equation in two-dimensional space. Consequently, two more wall boundary conditions should be required additionally.

Unlike the flow tangency condition that is mandatory to designate the inviscid wall, two other additional numerical wall boundary conditions may be somewhat flexible to select them. Kim et al. (2000) showed that the solution accuracy and stability of Roe's FDS may be affected by the way of choosing the additional two numerical wall boundary conditions.

The objective of this paper is to suggest robust wall boundary conditions in high-speed inviscid flowfield analysis. Four different sets of inviscid wall boundary conditions are proposed and then applied to solve the inviscid flowfield in high-speed flow regions. Since the boundary conditions may influence on the stability and accuracy of the numerical schemes used to solve the problems, three kinds of different upwind schemes which calculate the convection fluxes in Euler equation are considered; Steger-Warming's flux vector splitting (FVS), Roe's flux difference splitting (FDS), and Liou's hybrid upwind scheme called AUSM (advection upstream splitting method).

FVS concepts were introduced by Steger and Warming (1981). They split the flux vector into forward and backward contributions by splitting the eigenvalues of the Jacobian matrix of the flux into non-negative and non-positive groups. The split flux contributions are then spatially differenced according to one-sided upwind discretizations. The weak point of the flux vector splitting scheme of Steger-Warming is that the resulting flux vectors are not continuously differentiable at zeros of the eigenvalues (i. e. sonic and stagnation points). The lack of differentiability causes small oscillations, or glitches, at sonic points.

FDS concepts use the solution of the local Riemann problem. Roe, Osher and Godunov proposed various FDS schemes. Roe's FDS (Roe, 1981) is the most popular method among these FDS schemes because of its accuracy and efficiency. Roe's FDS gives very accurate solutions compared to FVS, however, this scheme has a shortcoming. Roe's FDS may yield nonphysical expansion shock waves and carbuncle phenomena in high-speed flow problems, especially near a stagnation region of a blunt body or a base region. Such defects can be removed by entropy fix (Harten, 1983). In this paper, however, no entropy fix is considered.

Liou and Steffen (1993) proposed a new flux splitting algorithm called AUSM that combines the efficiency of FVS and the accuracy of FDS. This scheme defines an appropriate cell interface advection Mach number then splits the fluxes for the convection terms based on the local Mach number. In spite of its accuracy and efficiency, AUSM has numerical overshoots behind the shock waves. AUSMD/V (Liou and Wada, 1994), AUSM+(Liou, 1996), and AUSMPW (Kim et al., 1998) schemes have been developed to eliminate undesired numerical results

successively.

2. Governing Equations

The conservative form of a two-dimensional compressible Euler equation in Cartesian coordinates system can be written as

$$\frac{\partial Q}{\partial t}+\frac{\partial F}{\partial x}+\frac{\partial G}{\partial y}=0 \tag{1}$$

where

$$Q=\begin{bmatrix}\rho\\ \rho u\\ \rho v\\ \rho E\end{bmatrix}\quad F=\begin{bmatrix}\rho u\\ \rho u^2+p\\ \rho uv\\ (\rho E+p)u\end{bmatrix}\quad G=\begin{bmatrix}\rho v\\ \rho uv\\ \rho v^2+p\\ (\rho E+p)v\end{bmatrix}$$

Q represents the conservative variables, and F and G represent the x-directional and y-directional convection terms, respectively. The choice of nondimensional parameters is arbitrary. Here the variables are nondimensionalized based on the free stream quantities.

3. Upwind Schemes

The x-directional convection flux vector F of each upwind scheme is shown in the following equations in Cartesian coordinates system. The y-directional convection flux vector G can be also constructed similarly.

3.1 Steger-Warming's FVS

Equation (2) represents the flux vector F in terms of the eigenvalues of its Jacobian matrix. More detailed information can be found in references (Steger and Warming, 1981).

$$F=\frac{\rho}{2\gamma}\begin{bmatrix}2(\gamma-1)\lambda_1+\lambda_3+\lambda_4\\ 2(\gamma-1)\lambda_1 u+\lambda_3(u+a)+\lambda_4(u-a)\\ 2(\gamma-1)\lambda_1 v+\lambda_3 v+\lambda_4 v\\ (\gamma-1)\lambda_1(u^2+v^2)+\frac{\lambda_3}{2}((u+a)^2+v^2)+\frac{\lambda_4}{2}((u-a)^2+v^2)+\frac{(3-\gamma)(\lambda_3+\lambda_4)a^2}{2(\gamma-1)}\end{bmatrix} \tag{2}$$

3.2 Roe's FDS

Equation (3) represents the flux vector F at the control volume boundary. Here the columns of S are the right eigenvectors of constant matrix that is selected based on local conditions shown in references (Roe, 1981).

$$F_{i+1/2}(Q_L, Q_R)=\frac{1}{2}((F_L+F_R)-S\,|\,\Lambda\,|\,S^{-1}\Delta Q) \tag{3}$$

where

$$S=\begin{pmatrix}1 & 0 & 1 & 1\\ \tilde{u} & 0 & \tilde{u}+\tilde{a} & \tilde{u}-\tilde{a}\\ \tilde{v} & \tilde{v} & \tilde{v} & \tilde{v}\\ (\tilde{u}^2+\tilde{v}^2)/2 & \tilde{v}^2 & \tilde{H}+\tilde{u}\tilde{a} & \tilde{H}-\tilde{u}\tilde{a}\end{pmatrix}\quad A=\begin{pmatrix}\tilde{u} & 0 & 0 & 0\\ 0 & \tilde{u} & 0 & 0\\ 0 & 0 & \tilde{u}+\tilde{a} & 0\\ 0 & 0 & 0 & \tilde{u}-\tilde{a}\end{pmatrix}$$

$$\tilde{u}=\frac{\rho_L^{1/2}u_L+\rho_R^{1/2}u_R}{\rho_L^{1/2}+\rho_R^{1/2}},\ \tilde{v}=\frac{\rho_L^{1/2}v_L+\rho_R^{1/2}v_R}{\rho_L^{1/2}+\rho_R^{1/2}},\ \tilde{H}=\frac{\rho_L^{1/2}H_L+\rho_R^{1/2}H_R}{\rho_L^{1/2}+\rho_R^{1/2}},\ \text{and}$$

$$\tilde{a}=(\gamma-1)\left[\tilde{H}-\frac{(\tilde{u}^2+\tilde{v}^2)}{2}\right]$$

3.3 Liou's AUSM

Equation (4) represents the flux vector F at the control volume boundary (Liou and Steffen, 1993).

$$F_{i+1/2}=F^{(c)}_{i+1/2}+p_{i+1/2} \tag{4}$$

where

$$F^{(c)}_{i+1/2}=M_{i+1/2}\begin{bmatrix}\rho a\\ \rho au\\ \rho av\\ \rho aH\end{bmatrix}_{L/R}$$

$$(\cdot)_{L/R}=\begin{cases}(\cdot)_L & \text{if } M_{i+1/2}\geq 0\\ (\cdot)_R & \text{if } M_{i+1/2}<0\end{cases}$$

$$M_{i+1/2}=M_L^{+}+M_R^{-}$$

Table 1 Wall boundary condition set

Case	Wall boundary conditions			
I	① $P_1=P_2$	② $H_1=H_\infty$	③ $(V_n)_1=0$	④ $(V_t)_1=(V_t)_2$
II	① $\rho_1=\rho_2$	② $(\rho E)_1=(\rho E)_2$	③ $(V_n)_1=0$	④ $(V_t)_1=(V_t)_2$
III	① $P_1=P_2$	② $H_1=H_2$	③ $(V_n)_1=0$	④ $(V_t)_1=(V_t)_2$
IV	① $P_1=P_2$	② $(\rho E)_1=(\rho E)_2$	③ $(V_n)_1=0$	④ $(V_t)_1=(V_t)_2$

$$M^{\pm}=\begin{cases}\pm\frac{1}{4}(M\pm1)^2 & \text{if } |M|\le 1\\ \frac{1}{2}(M\pm|M|) & \text{if } |M|>1\end{cases}$$

and

$$p_{i+1/2}=\begin{bmatrix}0\\ p\\ 0\\ 0\end{bmatrix}$$

$$p_{i+1/2}=p_L^{+}+p_R^{-}$$

$$p^{\pm}=\begin{cases}\frac{p}{4}(M\pm1)^2(2\mp M) & \text{if } |M|\le 1\\ \frac{p}{2}(M\pm|M|)/M & \text{if } |M|>1\end{cases}$$

4. Inviscid Wall Boundary Condition

As mentioned above, four wall boundary conditions are necessary to solve a two-dimensional Euler equation. One of them is the flow tangency condition. This condition provides two wall boundary conditions. In other words, the normal component of velocity on the wall is zero and the tangential component of velocity is parallel to the wall surface. Two more wall boundary conditions, therefore, should be prepared additionally.

In general, one of the preferred wall boundary conditions is the pressure boundary condition in inviscid flow calculation. The pressure on the wall can be extrapolated from the pressure at the first node point away from the wall if the grid size between these two points is very small and the normal pressure gradient at node point away from the wall is also very small. Instead of pressure extrapolation, density, total enthalpy, or total energy may be considered as an extrapolation parameter. In this study, four different sets of wall boundary conditions are proposed as shown in Table 1. Each set of wall boundary conditions includes the flow tangency condition commonly. The subscript 1 and 2 represent the parameter quantity on the wall and at the first node point away from the wall, respectively. The subscript ∞ represents the free stream condition.

5. Euler Solver Development

A two-dimensional compressible Euler solver has been developed. The Euler solver solves a conservative form of the Euler equation using a finite volume method in curvilinear coordinates system, and has the capability to handle a multi-block grid topology that can reduce the difficulties in generating a grid for a complex geometry.

The inviscid fluxes are calculated by Steger-Warming's FVS, Roe's FDS or Liou's AUSM. Using the MUSCL approach with Albada's flux limiter preserves the second order accuracy in space. In this paper, however, the first order accuracy was applied to solve the flowfield. Beam-Warming's approximate factorization implicit scheme is used to increase the time step margin. Also, the implicit boundary conditions are included.

The Euler solver was validated by analyzing the flowfield around the NACA 0012 airfoil at $M_\infty=0.75$, $\alpha=2.0°$ and $M_\infty=0.80$, $\alpha=1.25°$ (Kim, 2000 & Kim et al., 2000).

6. Numerical Results and Discussion

A grid shown in Fig. 1 was generated algebraically to analyze a high-speed inviscid flow around a quarter circle geometry in the range of $M_\infty=2.0$ to 6.0.

Four different sets of wall boundary conditions

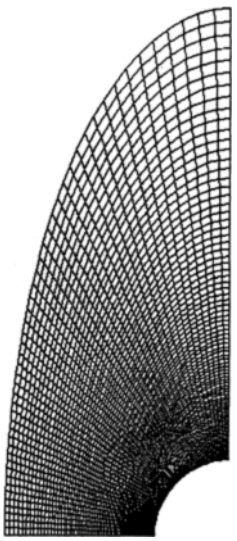

Fig. 1 Quarter circle geometry grid (50×100)

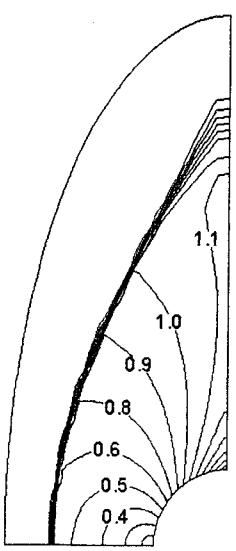

Fig. 2 Mach contour (M_∞=2.0)

shown in Table 1 were applied to three different upwind schemes to figure out what is the most robust wall boundary condition set.

As a matter of convenience, only typical Mach contours are plotted. For example, Fig. 2 shows a Mach contour obtained by Roe's FDS at M_∞=2.0. This figure will be used to represent a numerical result that was obtained by Steger-Warming's FVS or Liou's AUSM at M_∞=2.0 if those results have very similar contour line distributions,

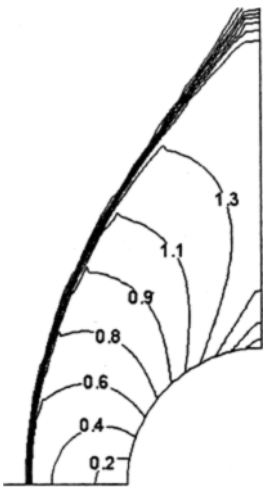

(a) Normal contour

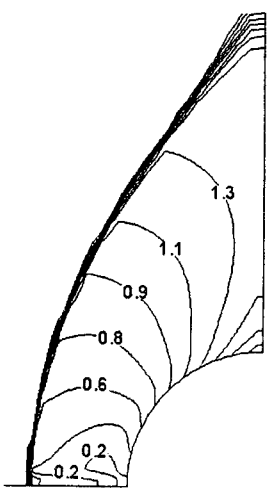

(b) Wiggled contour

Fig. 3 Mach contour (M_∞=3.0)

even though the detailed accuracy is somewhat different depending on the upwind schemes. This means that we have an interest in the overall accuracy of the numerical solution instead of detailed accuracy through this paper.

When the first wall boundary condition set, Case I, was applied to the Steger-Warming's FVS at M_∞=2.0, a reasonable shock could be formed as shown in Fig. 2. This boundary condition set also yielded reasonable Mach contours at M_∞=3.0 ~6.0 (Fig. 3(a), 4(a), 5(a), and 6 (a)).

For Roe' FDS, a reasonable Mach contour could be formed at low Mach number, M_∞=2.0

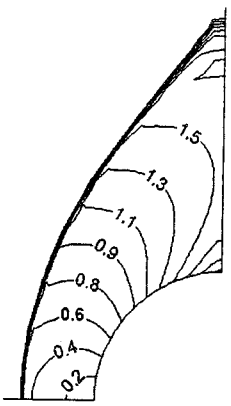

(a) Normal contour

(b) Carbuncle phenomenon

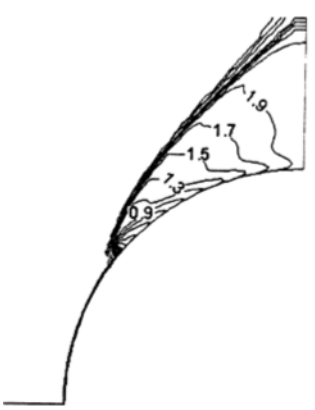

(c) Nonphysical shock

Fig. 4 Mach contour (M_∞=4.0)

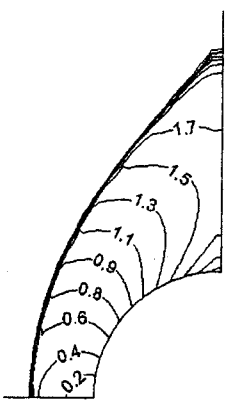

(a) Normal contour

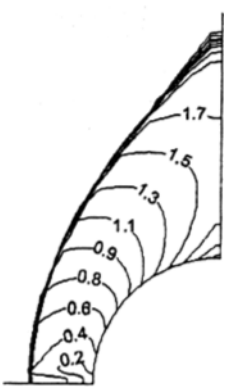

(b) Wiggled contour

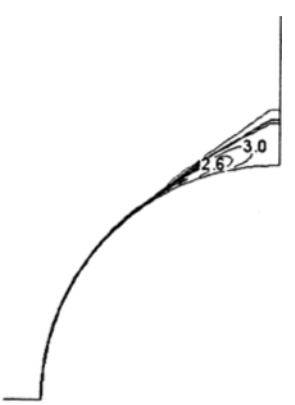

(c) Nonphysical shock

Fig. 5 Mach contour (M_∞=5.0)

(Fig. 2). The defect of Roe's FDS was observed near the stagnation region at M_∞=3.0 (Fig. 3(b)). However, this kind of defect does not hurt overall accuracy of the Roe solution. This wall boundary condition set, however, could not generate a physically correct shock anymore at higher Mach number than M_∞=4.0 (Fig. 4(c), 5(c), and 6(c)) even though residuals decreased up to the machine accuracy.

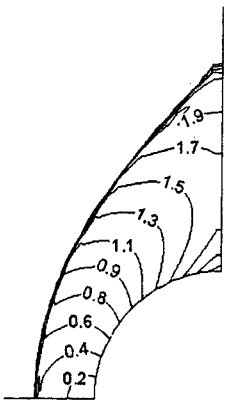

(a) Normal contour

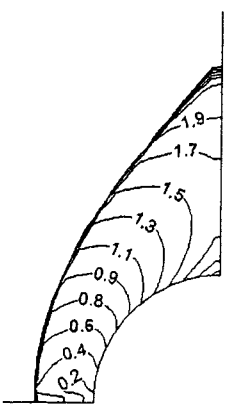

(b) Wiggled contour

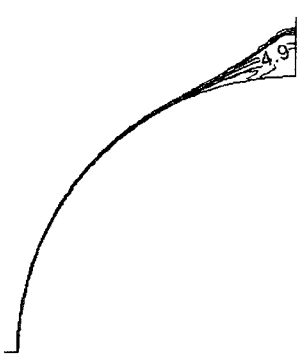

(c) Nonphysical shock

Fig. 6 Mach contour (M_∞=6.0)

Almost same tendency was observed when Liou's AUSM was used. Reasonable shocks could be obtained at low Mach numbers, M_∞=2.0 (Fig. 2) and 3.0 (Fig. 3(a)). However, no correct solution could be obtained at higher Mach numbers than M_∞=4.0 (Fig. 4(c), 5(c), and 6(c)).

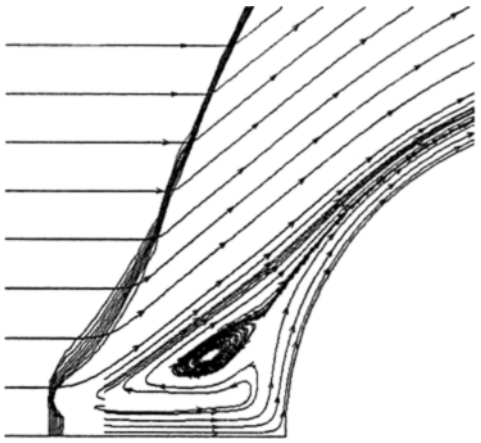

Fig. 7 Particle traces (M_∞=4.0, Roe's FDS)

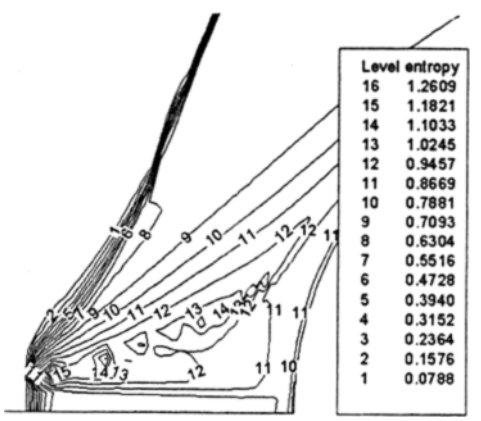

Fig. 8 Entropy contour (M_∞=4.0, Roe's FDS)

Therefore, it could be said that Case I is good for only Steger-Warming's FVS.

On the contrary, the second wall boundary condition set, Case II, had no problem to generate a physically correct shock in the whole test range of Mach numbers when Steger-Warming's FVS or Liou's AUSM was used (Fig. 2, 3(a), 4(a), 5 (a), and 6 (a)).

For Roe's FDS, however, this wall boundary condition set gave various numerical solutions depending on the flow speed. A reasonable shock was formed at low Mach number, M_∞=2.0 (Fig. 2). Some wiggled contour line distributions near the stagnation region were observed at M_∞=3.0 (Fig. 3(b)) and 5.0 (Fig. 5(b)) whereas a carbuncle

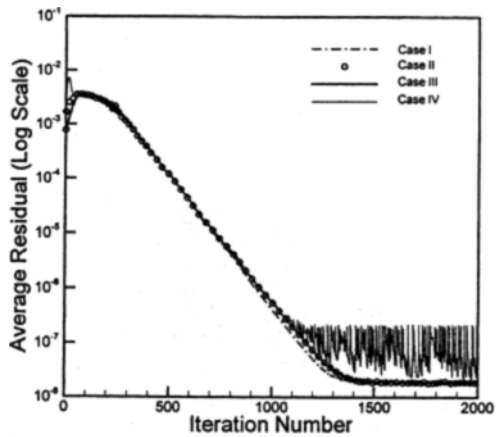

Fig. 9 Convergence history (M_∞=3.0, SW's FVS)

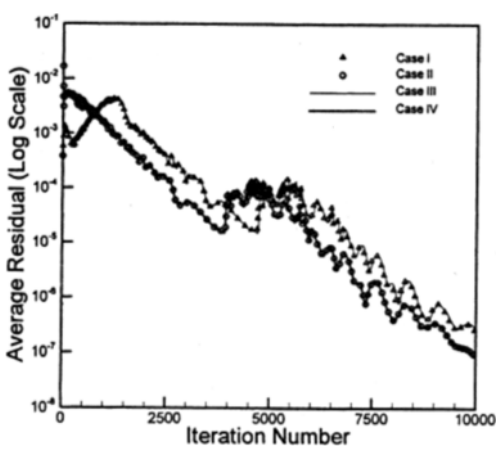

Fig. 10 Convergence history (M_∞=3.0, Roe's FDS)

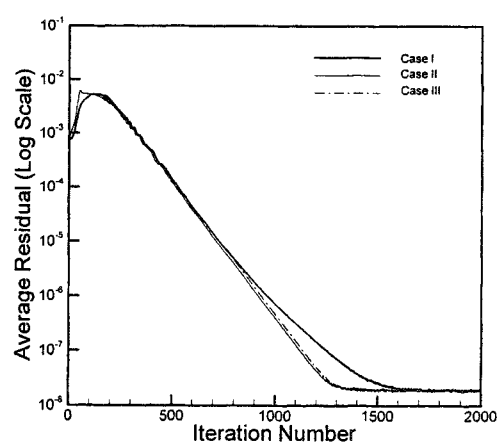

Fig. 11 Convergence history (M_∞ =3.0, Liou's AUSM)

phenomenon appeared at M_∞=4.0 (Fig. 4(b)). The carbuncle phenomenon is a typical defect of Roe solution. This nonphysical phenomenon is plotted again in Figs. 7~8. Figure 7 shows particle traces, which cannot occur in real physics. This nonphysical situation occurred because of decreasing entropy near the stagnation region as shown in Fig. 8. Using entropy fix although solution accuracy is degraded a little can eliminate a carbuncle phenomenon or wiggled contour line distributions near the stagnation region. No correct solution was obtained at higher Mach numbers than M_∞=6.0 (Fig. 6(c)).

Therefore, Case II is considered as a recommendable wall boundary condition set when Steger-Warming's FVS or Liou's AUSM is used. However, Case II is not good for Roe's FDS.

The third wall boundary condition set, Case III, had exactly same tendency as Case I.

The last wall boundary condition set, Case IV, was really bad for Liou's AUSM. Only valid shock was obtained at M_∞=2.0 (Fig. 2). At higher Mach numbers than M_∞ =3.0, no converged solution could be obtained. Case IV, however, could be considered as a recommendable wall boundary condition set for both Steger-Warming's FVS and Roe's FDS.

There was no problem to generate a correct shock in the whole test range of Mach numbers (Fig. 2, 3(a), 4(a), 5(a), and 6 (a)) for Steger-Warming's FVS.

However, some wiggled contour lines near the stagnation point were observed at M_∞=3.0 (Fig. 3(b)) and higher than 5.0 (Fig. 5(b) and Fig. 6 (b)) for Roe's FDS. But the overall Mach contour looks reasonable. Moreover, an accurate numerical solutions were obtained at M_∞=2.0 and 4.0 (Fig. 2 and Fig. 4(a)). In case of considering entropy fix to remove the defects of Roe solution, Case IV is still the best choice among four sets of wall boundary conditions because Case IV can minimize the diffusion effect of entropy fix compared to others.

Figures 9~11 show the convergence histories at M_∞=3.0, which were obtained by implicit method for both Steger-Warming's FVS and

Table 2 Mach contours summary (Steger-Warming's FVS)

	Case I	Case II	Case III	Case IV
M_∞=2.0	Fig. 2	Fig. 2	Fig. 2	Fig. 2
M_∞=3.0	Fig. 3(a)	Fig. 3(a)	Fig. 3(a)	Fig. 3(a)
M_∞=4.0	Fig. 4(a)	Fig. 4(a)	Fig. 4(a)	Fig. 4(a)
M_∞=5.0	Fig. 5(a)	Fig. 5(a)	Fig. 5(a)	Fig. 5(a)
M_∞=6.0	Fig. 6(a)	Fig. 6(a)	Fig. 6(a)	Fig. 6(a)

Table 3 Mach contours summary (Roe's FDS)

	Case I	Case II	Case III	Case IV
M_∞=2.0	Fig. 2	Fig. 2	Fig. 2	Fig. 2
M_∞=3.0	Fig. 3(b)	Fig. 3(b)	Fig. 3(b)	Fig. 3(b)
M_∞=4.0	Fig. 4(c)	Fig. 4(b)	Fig. 4(c)	Fig. 4(a)
M_∞=5.0	Fig. 5(c)	Fig. 5(b)	Fig. 5(c)	Fig. 5(b)
M_∞=6.0	Fig. 6(c)	Fig. 6(c)	Fig. 6(c)	Fig. 6(b)

Table 4 Mach contours summary (Liou's AUSM)

	Case I	Case II	Case III	Case IV
M_∞=2.0	Fig. 2	Fig. 2	Fig. 2	Fig. 2
M_∞=3.0	Fig. 3(a)	Fig. 3(a)	Fig. 3(a)	No solution
M_∞=4.0	Fig. 4(c)	Fig. 4(a)	Fig. 4(c)	No solution
M_∞=5.0	Fig. 5(c)	Fig. 5(a)	Fig. 5(c)	No solution
M_∞=6.0	Fig. 6(c)	Fig. 6(a)	Fig. 6(c)	No solution

Liou's AUSM and by explicit method for Roe's FDS. These plots show the effect of four different wall boundary condition sets on the solution convergence rate. Case I, II, and III shown in Fig. 9 gave very similar stable convergence histories whereas Case IV gave a strong oscillatory convergence history at low-level residuals when Steger-Warming's FVS was used. It means that Case IV may be an inadequate wall boundary condition set from the viewpoint of stability.

When Roe' FDS was used, the convergence histories had periodic oscillations for all boundary condition sets as shown in Fig. 10. In this figure, we found that Case II and IV gave lower magnitude of residual than other wall boundary condition sets at the same iteration number.

The convergence rates were compared in Fig. 11 when Liou's AUSM was used. Case II and III showed very similar convergence rates whereas Case I showed the minimum convergence rate.

Tables 2~4 summarize the above discussions concisely again and the most robust wall boundary condition set for each upwind scheme is marked with dark region in Tables 2~4.

7. Conclusion

Four different sets of inviscid wall boundary conditions are proposed and then applied to high-speed flowfield analysis around a quarter circle geometry body.

It is found that the way of choosing the numerical wall boundary conditions affects strongly the stability and accuracy of the numerical schemes in high-speed flow calculation although it may not be serious at low-speed flow region.

Any kind of wall boundary condition sets except Case IV is recommendable when Steger-Warming's FVS is used to calculate the convection fluxes. Case IV is the most robust wall boundary condition set for Roe's FDS whereas it is the worst boundary condition set for Liou's AUSM. Case II is strongly recommended as the most robust wall boundary condition set for Liou's AUSM.

These proposed wall boundary conditions yield physically correct solutions as well as the maximum

convergence rates in high-speed flow calculation.

The above conclusion, however, may be valid for the case considered in this study. Therefore, further study will be accomplished to generalize the conclusion.

References

Chakravarthy, S.R., Anderson, D. A., and Salas, M. D., 1980, "The Split-Coefficient Matrix Method for Hyperbolic Systems of Gas Dynamic Equations," AIAA Paper 80-0268.

Cho, Ji Ryong, 1997, "A Convection Scheme Sensitized to the Convection Direction of a Scalar Quantity," *KSME International Journal*, Vol. 11, No. 1, pp. 106~114.

Harten, A., 1983, "High Resolution Schemes for Hyperbolic Conservation Laws," *Journal of Computational Physics*, Vol. 49, pp. 357~393.

Kim, K.H., Lee, J.H., and Rho, O.H., 1998, "An Improvement of AUSM Schemes by Introducing the Pressure-Based Weight Functions," *Computer & Fluids*, Vol. 27, No. 3, pp. 311~346.

Kim, M.S., 2000, "A Comparative Study of Different Upwind Schemes in Inviscid Transonic and Supersonic Flowfields," *Journal of the Korean Society for Aeronautical and Space Sciences*, Vol. 28, No. 2, pp. 26~34.

Kim, M.S. and Kim, H.K., 2000, "An Investigation of Characteristics of Roe's FDS by Using the Compressible Euler Equations," *Journal of the Korean Society for Aeronautical and Space Sciences*, Vol. 28, No. 7, pp. 1~9.

Liou, M.S., 1996, "A Sequel to AUSM: AUSM+," *Journal of Computational Physics*, Vol. 129, pp. 364~382.

Liou, M.S. and Steffen Jr. C.J., 1993, "A New Flux Splitting Scheme," *Journal of Computational Physics*, Vol. 107, pp. 23~39.

Liou, M.S. and Wada, Y., 1994, "A Flux Splitting Scheme with High-Resolution and Robustness for Discontinuities," AIAA Paper 94-0083.

Moretti, G., 1979, "The λ-Scheme," *Computer and Fluids*, Vol. 7, pp. 191~205.

Roe, P.L., 1981, "Approximate Riemann Solvers, Parameter Vectors and Difference Schemes," *Journal of Computational Physics*, Vol. 43, pp. 357~372.

Steger, J.L. and Warming, R.F., 1981, "Flux Vector Splitting of the Inviscid Gasdynamics Equations with Application to Finite Difference Methods," *Journal of Computational Physics*, Vol. 40, pp. 263~293.